

Influence of Grinding Ball-Motion Behavior on Particle Crushing Performance and a Way of Micro-particle Preparation in a Flutter Ball Mill

LIANG Man¹, SUN Weihong¹, SUN Yi^{2*}, SHAN Jihong²

1. College of Mechanical and Electrical Engineering, China Jiliang University, Hangzhou 310018, P.R.China;

2. College of Mechanical Engineering, Zhejiang University of Technology, Hangzhou 310014, P.R.China

(Received 10 March 2020; revised 10 July 2020; accepted 1 September 2020)

Abstract: Motion behavior of grinding balls plays a vital role in improving efficiency of particle crushing. A method of preparing micro-particles by changing ball-motion behavior in a flutter mill is proposed and multiple grinding experiments are conducted. Crushing performance parameters, such as breakage rate S_i , production rates of fine particles F_i and F_i^* , are studied in different motion conditions. From the results, a better crushing performance is attained in the coupled motion modes of rotating speed ratio of 85%, with a vibrating amplitude of 8 mm and a frequency of 12 Hz. In addition, the influence of ball-motion behavior on particle crushing performance is discussed. The ball-motion behaviors, such as the collision energy loss E , among grinding balls have some relationship with the particle crushing performance of S_i . Therefore, this study not just provides an efficiency way of accumulating micro-particles, but also reveals how the ball-motion behavior influence particle crushing performance in the flutter mill.

Key words: flutter ball mill; ball-motion behavior; breakage rate; collision energy loss; micro-particle preparation

CLC number: TD453

Document code: A

Article ID: 1005-1120(2021)03-0450-12

0 Introduction

Many modern technologies used today rely on the preparation of micro-particles, such as ceramic industries, chemical product, 3D printing and so on. These industries require billions of tons of metallic ores, cement, minerals, and other solid particles and ball milling is the most important mechanical treatment used to reduce the particle size^[1]. Fine powders with the size of submicron are urgently required in preparing high-quality products, but a large amount of electrical energy ranging from 5 kWh/t to 50 kWh/t is consumed in the milling processes due to the low energy utilization^[2]. Effective crushing behavior of ball-motion can bring fine powders by consuming only a little amount of energy^[3]. Many scholars pay much attention to improve

and change the method of ball-motion behavior in order to accumulate micro-particles^[4-6]. For example, the structure of mill cylinder has been altered by adding different stirring rods, paddles or liners to enhance grinding behavior of ball-motion like the stirred mill, two-way rotating ball mill^[7-12]. Thus, the motion mode of mill has been changed by transforming mill motion or adding other motions, such as vibration, planetary, or flutters^[13-17].

There are a number of reports on the effect of motion behavior of grinding balls on the crushed performance of particles. Gupta et al.^[18] studied the force condition and kinematic equation of a single grinding ball. Fan et al.^[19] recommended a theoretical model on the motion area of a group of grinding balls, supplementing the ball-motion function in a complex condition. Cleary and Powell et al.^[20-21] dis-

*Corresponding author, E-mail address: sunyi@zjut.edu.cn.

How to cite this article: LIANG Man, SUN Weihong, SUN Yi, et al. Influence of grinding ball-motion behavior on particle crushing performance and a way of micro-particle preparation in a flutter ball mill[J]. Transactions of Nanjing University of Aeronautics and Astronautics, 2021, 38(3):450-461.

<http://dx.doi.org/10.16356/j.1005-1120.2021.03.009>

cussed on the influence of many factors including rotating speed ratio, filling rate, and balls' size on the alteration of ball-motion behavior. Some researchers concluded that different motion behaviors of grinding balls affect the milling process, crushing ways of impacting and grinding, and crushing zones^[22]. A better motion behavior should involve a reasonable proportion of the two crushing ways to improve milling efficiency as well as accumulating micro-particles^[23]. Thus, the division of motion regions for the grinding balls were carried out earlier and we analyzed the ball-motion behavior in different conditions by changing motion parameters in a flutter ball mill^[24]. However, the influence of changing the ball-motion behavior on the crushing performance of ground particles in the flutter mill is still unclear; and motion behavior of balls is totally available by understanding the simulation software of discrete element method (DEM)^[25], the crushing conditions of ground particles in actual grinding experiments haven't carried out till now. Moreover, if the crushing performance of ground particles have some relation with the ball-motion behavior which can be obtained from numerical simulation, time and cost of milling processes may be dramatically reduced.

Therefore, ball-motion behavior can influence the crushing performance of ground particles obviously, as is focused in this report. This paper describes the way of micro-particle preparation in a flutter ball mill in different motion conditions. Then, numerical simulation of the grinding balls is conducted for analysis the ball-motion behavior to study how it influences particle crushing performance and the more efficiency way of accumulating micro-particles.

1 Experiments of Preparing Micro-particles

The flutter ball mill is a novel milling equipment combined with the two coupled motions of horizontal rotation and vertical vibration, which can change the ball-motion behavior and reduce the weak zone efficiently in a milling process^[26-28]. Fig.1

shows a schematic diagram of a flutter ball mill^[17]. There are two different motors to drive the mill cylinder and change the ball-motion behavior by adjusting three motion parameters including rotating speed ratio, vibrating amplitude, and frequency.

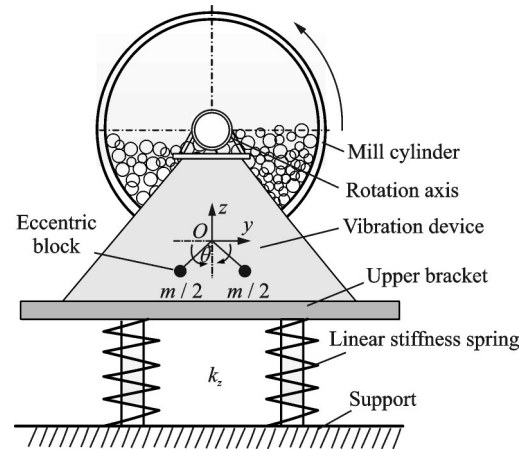


Fig.1 A schematic diagram of a flutter ball mill^[17]

1.1 Experimental set-up and simulation model

Fig.2 shows the experimental mill set-up. It implements the change of motion behavior of balls caused by the varied motion parameters. The operating conditions and physical characteristics are described in Table 1. The feed material in the mill is silica sand, provided from Zhejiang Dingchuang Silica Sand Co., and its initial particle size is 0.4—0.85 mm, as its chemical composition is shown in Table 2. The silica sand is comprised of SiO₂ (86% of the weight), Al₂O₃ (1.2% of the weight), Fe₂O₃ (1.1% of the weight), NaO (1.3% of the weight), and other components (about 10% of the weight).

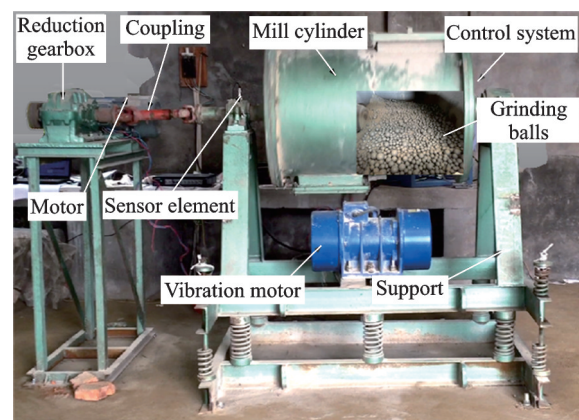


Fig.2 Experimental set-up of the flutter ball mill

Table 1 Experimental operating conditions and physical characteristics of the flutter mill

Parameter	Value ^[24]
Diameter of the shell / mm	600
Length of the shell / mm	450
Internal volume / cm ³	123 028.7
Filling ratio / %	45
Ball size / mm	∅20:∅16:∅10
Size distribution	3:6:1
Vibration mode	Vertical
Feed	Silica sand
Density / (kg·m ⁻³)	2 650
Void ratio / %	60
Mass of the feed / kg	35.2

Table 2 Chemical composition of the used silica sand

Constituent	SiO ₂	Al ₂ O ₃	Fe ₂ O ₃	MgO	CaO	NaO	Others
Weight percentage / %	86	1.2	1.1	0.8	0.4	1.3	9.2

The vibrating motion of mill cylinder is well-traced by a sensor element in Fig.2. When a vibrating amplitude of 4 mm is adjusted, the displacement of the point on *Z* and *Y* axes are obtained after several cycles, as shown in Fig.3 (a). The maximum wavy distance on the *Z* axis is about 4 mm with an unavoidable wavy distance of about 1 mm on the *Y* axis, within the allowable error. The trajectory of the cylinder is shown in Fig.3(b), and its amplitude is almost the same with the selected value.

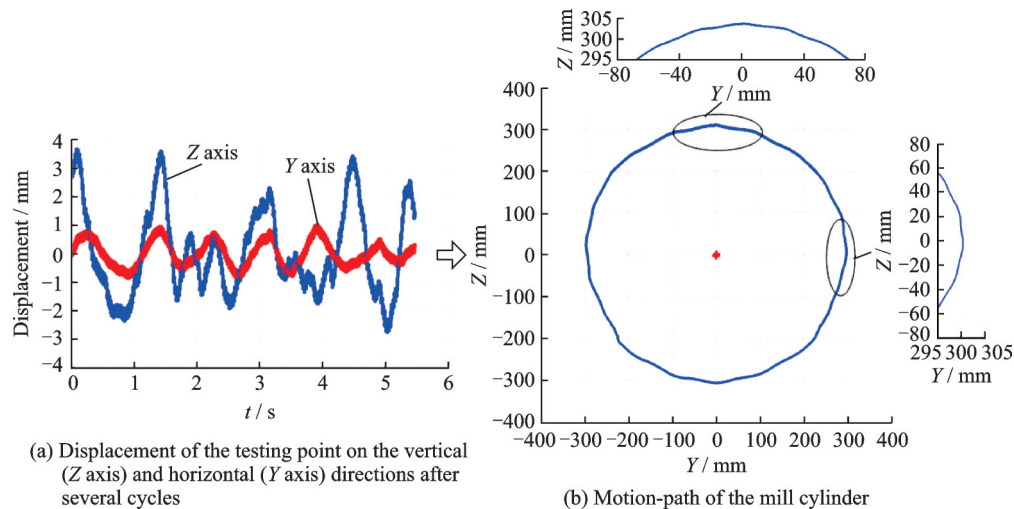


Fig.3 Testing results for the experimental set-up with the vibrating amplitude of 4 mm

The simulation process in EDEM contains three parts involving building a computational model for the flutter mill, generating particles in the cylinder, and imposing coupled motions to the mill. The completed situational model is shown in Fig.4 (a). The parameters in simulation model are represented in Table 3 and a tagged point on the shell is

Table 3 Simulation parameters in EDEM model

Parameter	Ball	Wall
Material	Steel	Steel
Density / (kg·m ⁻³)	7 800	7 800
Shear modulus / 10 ¹⁰ Pa	6.18	24.6
Poisson's ratio	0.27	0.22
Coefficient of restitution	0.5	0.56
Static friction coefficient	0.4	0.15
Rolling friction coefficient	0.05	0.15
Simulation time step / s	$\leq 1 \times 10^{-3}$	

shown in Fig.4(b). The trajectory of the tagged point is obtained after several cycles, as shown in Fig.4(c), which is close to the experimental set-up value.

1.2 Experimental design

The following three coupling level motion parameters were selected. Rotating speed ratio and vibrating amplitude were chosen as 65%, 75%, and 85% and 4, 6, and 8 mm at the frequencies of 4, 8, and 12 Hz, respectively^[29]. Then, an effective optimal design scheme of uniformly orthogonal plan^[30] was used to deduce the experimental group numbers. The experimental scheme and three parameters in each group are displayed in Table 4. To compare with the coupled motion, the tenth group of rotating motion only is added as the con-

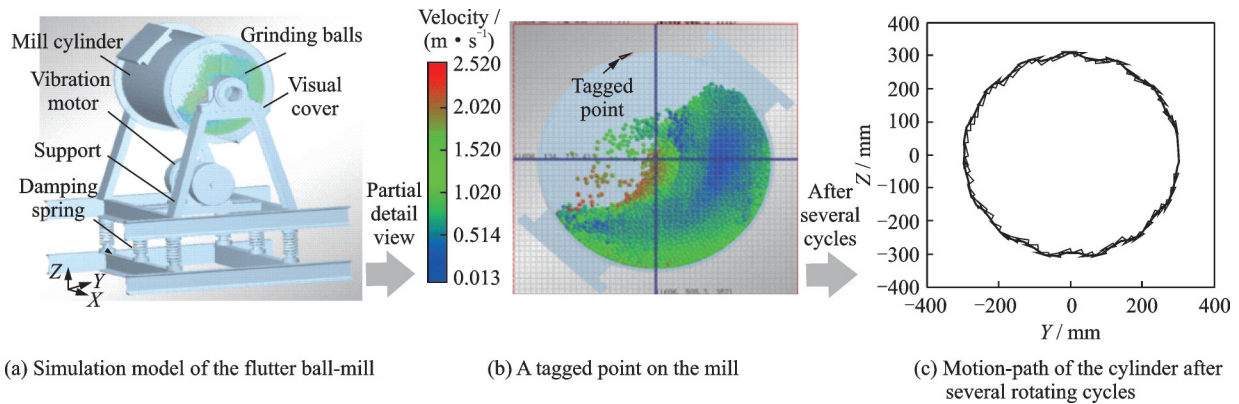


Fig.4 Simulation model and the motion-path of the cylinder

Table 4 Orthogonal test table

Group number	Rotation speed ratio / %	Amplitude / mm	Frequency / Hz	Motion mode
1	65	4	4	Coupled motion
2	65	6	8	
3	65	8	12	
4	75	4	12	
5	75	6	4	
6	75	8	8	
7	85	4	8	
8	85	6	12	
9	85	8	4	
10	85	0	0	Rotation

trol group.

When the milling process ends, the specific surface area of ground particles is tested by an ASAP2020 Surface Area Instrument. Then, the particle size distribution is analyzed by a Malvern Laser Particle Size Analyzer.

2 Crushing Performance of Ground Particles

2.1 Particle size distribution

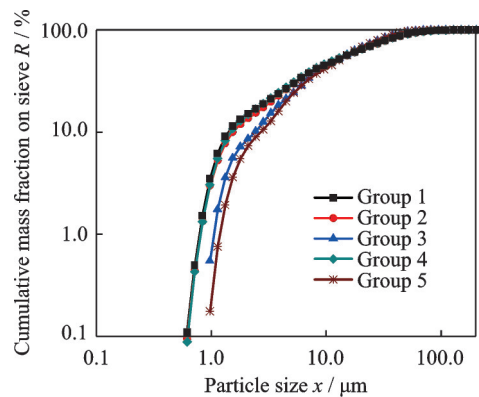
Fig.5 shows the ground particle size distribution in different motion conditions. The curves is fitted by linear regression analysis, and the linear fitting equations match Rosin Rammler Bennet (RRB) equation completely, as shown in^[31]

$$R = 100e^{-(x/x_0)^n} \quad (1)$$

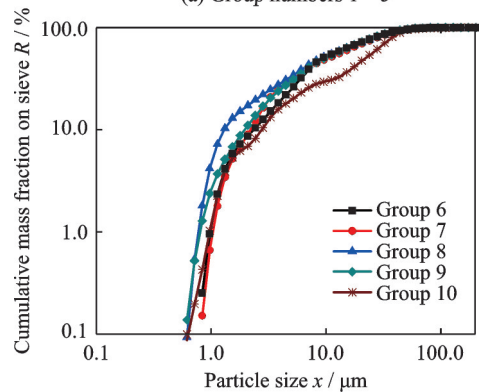
or

$$\ln [\ln (100/R)] = n \ln x - n \ln x_0 \quad (2)$$

where R is the cumulative mass fraction on a sieved mesh, x_0 the characteristic diameter that stands for the particle size, and n the uniformity coefficient



(a) Group numbers 1—5



(b) Group numbers 6—10

Fig.5 Fine particle-size distribution in different motion conditions

that stands for the width of particle size distribution. It should be noted that a small n leads to a wider particle size distribution^[32-33].

The RRB distribution function of the ground particles processed in each group is obtained based on Eq.(2). The characteristic particle size x_0 and uniformity coefficient n are summarized in Table 5. x_0 is decreased gradually with enhancing group numbers, except for group 10. It indicates that

the ground particles in coupled motions are uniformly refined because the ball-motion behaviors are preferred to accumulate micro-particles. However, the irregular uniformity coefficient, n , indicates that in some groups, micro-particles began to aggregation in a granular manner^[34]. Therefore, intensity of the coupled motions may significantly affect generation and accumulation of micro-particles.

Table 5 RRB liner regression results for the ground particles

No.	Rosin-Rammler distribution function	$x_0/\mu\text{m}$	n
1	$\ln[\ln(100/R)]=0.85\ln x-2.53$	20.030	0.85
2	$\ln[\ln(100/R)]=0.83\ln x-2.50$	19.600	0.83
3	$\ln[\ln(100/R)]=1.12\ln x-3.24$	19.326	1.12
4	$\ln[\ln(100/R)]=0.88\ln x-2.60$	18.020	0.88
5	$\ln[\ln(100/R)]=1.1\ln x-3.18$	18.057	1.10
6	$\ln[\ln(100/R)]=0.98\ln x-2.72$	17.032	0.98
7	$\ln[\ln(100/R)]=1.08\ln x-3.06$	16.100	1.08
8	$\ln[\ln(100/R)]=0.9\ln x-2.50$	16.080	0.90
9	$\ln[\ln(100/R)]=1.0\ln x-2.78$	16.120	1.00
10	$\ln[\ln(100/R)]=0.95\ln x-3.22$	29.563	0.95

2.2 Production rate of fine particles

The production rate of fine particles, F_i , in different groups is inspected to study the crushing performance of particles in the flutter mill. The mass fraction of ground particles finer than the size of x_i at the time t is denoted as $F_i(t)$. The production rate of particles with sizes finer than 325, 650, and 1 600 mesh (F_{325} , F_{650} , F_{1600})^[35] is selected as the desired size, as shown in Figs.6—8.

The values of F_{325} are increased rapidly with enhancing the grinding time, as shown in Fig.6. Slopes of the fitting curves show the mean growth-rate of the micro-particles. They are smaller in groups 1—4 than that in groups 5—9. And the same changes of F_{650} and F_{1600} are obtained in Figs.7 and 8 except for their values. Finally, the values of F_{325} , F_{650} , and F_{1600} are compared in different groups after grinding for 120 min, as shown in Fig.9.

From Fig.9, it can be envisaged that a little volatility, but with a steady increase is attained for F_{325} , F_{650} , and F_{1600} with enhancing of the group

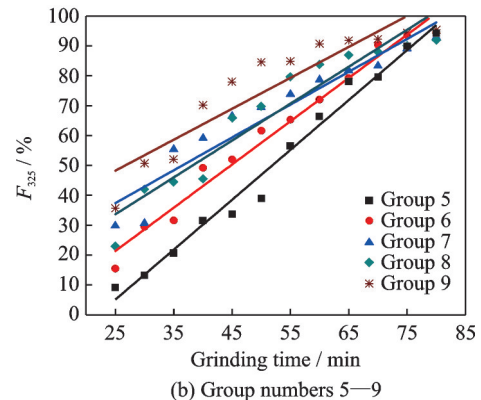
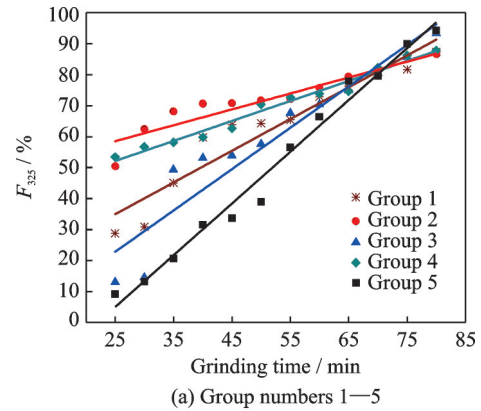
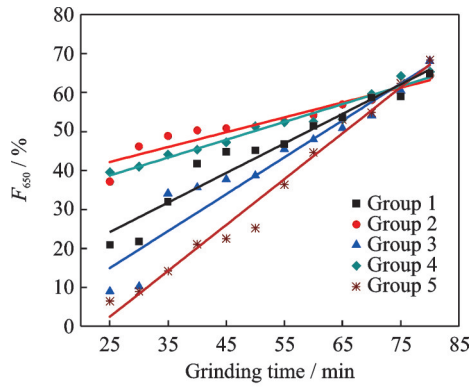
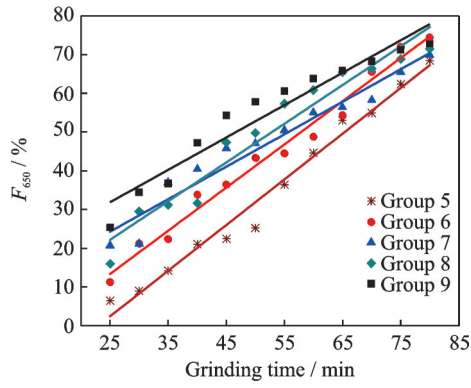


Fig.6 Variation of F_{325} of particles with a size finer than 325 mesh

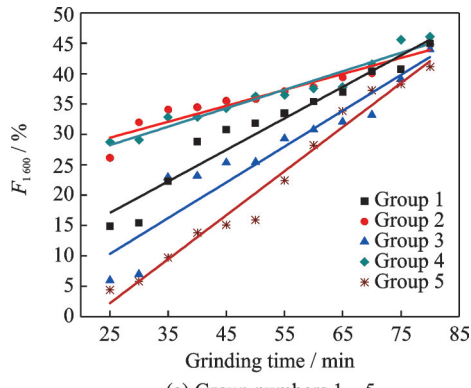


(a) Group numbers 1—5

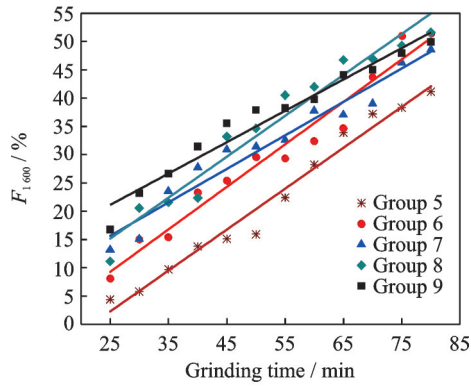


(b) Group numbers 5—9

Fig.7 Variation of F_{650} of particles with a size finer than 650 mesh



(a) Group numbers 1—5



(b) Group numbers 5—9

Fig.8 Variation of F_{1600} of particles with a size finer than 1 600 mesh

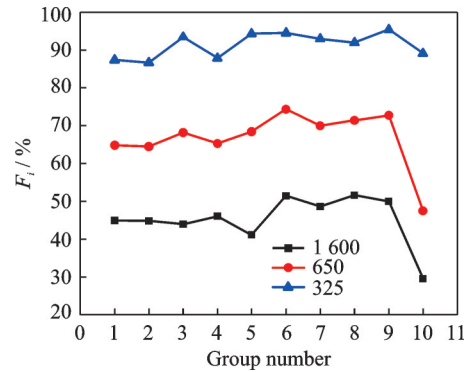


Fig.9 Comparison of F_{325} , F_{650} , and F_{1600} in all groups

numbers, except for group 10, in which a much smaller value of F_{650} and F_{1600} is gained.

Considering the energy consumed by the flutter mill during milling process, the production rate of fine particles per unit power, F_i^* , can be defined as^[18]

$$F_i^* = (dF_i(t)/dt)(M/P) \quad (3)$$

where M , t , and P are the mass of feed particles, grinding time, and net power drawn by mill, respectively. Fig.10 provides the values of F_i^* in the flutter mill and shows the energy consumption during milling process. F_i^* is changed significantly in different groups and has a sharp drop in the groups 2 and 4.

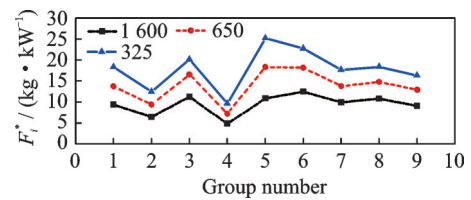


Fig.10 Values of F_i^* in the flutter-motion conditions

2.3 Particles breakage rate

According to the first-order grinding dynamics, $M_i(0)$ and $M_i(t)$ denote the mass fraction of particle size (i) before and after grinding for t min, respectively. Actually, i is ranged from 0.4 mm to 0.65 mm, confirming approximately no change in size. The data obtained from results in each group are fitted with the mass fraction of crushed particles, which is described according to^[36]

$$M_i(t) = M_i(0) \exp(-S_i t) \quad (4)$$

where S_i is the breakage rate of the feed size (i). As it is often the case, for $i=1$, Eq.(4) can be rewritten as^[37]

$$\ln \frac{M_1(t)}{M_1(0)} = \frac{-S_1 t}{2.3} \quad (5)$$

The dependence of $\ln[M_i(t)/M_i(0)]$ with t along with the corresponding fitting curves are shown in Fig.11. The distribution of curves in Fig.11(a) is almost similar and the corresponding slopes are little changed. However, more different curves are attained in Fig.11(b). Based on Eq.(5), the value of specific breakage rate, S_1 , can be derived from fitting curves, as shown in Fig.12. S_1 is increased continually with group numbers until group 8, where reaches up to the maximum value

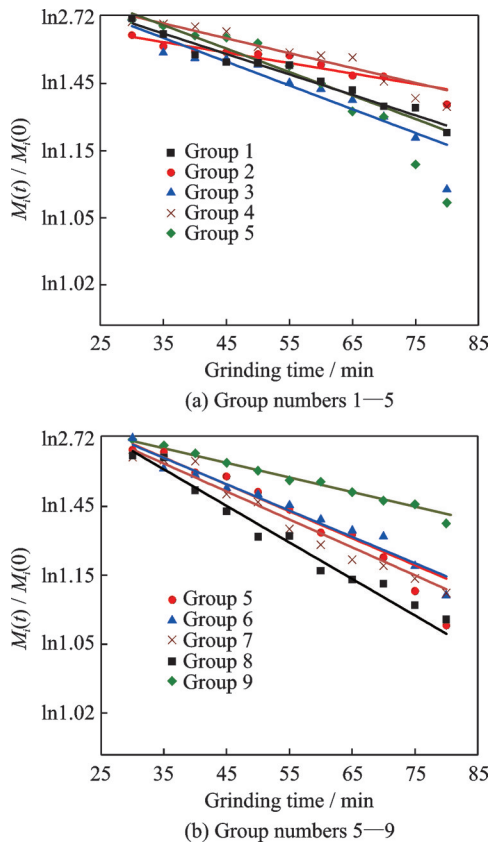


Fig.11 First-order grinding dynamic plots for ten groups

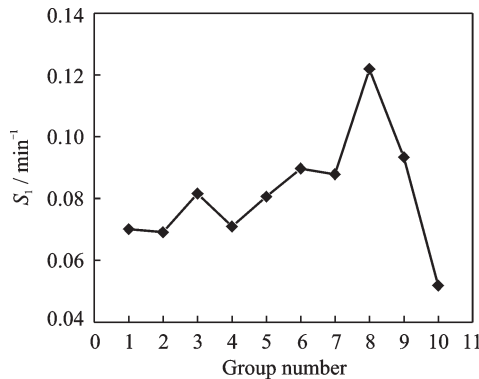


Fig.12 Variation of particle breakage rate S_1 in ten groups

of 0.12. These findings confirm that this motion condition has a strong ability to break the feed particles.

3 Motion Behavior of Grinding Balls in Numerical Simulation Results

3.1 Mean contact force

Mean contact force, F_{mcf} , is the mean value of stress when collision occurs between balls and wall. The parameter describes the impact and friction forces affecting ground particles. F_{mcf} among balls in the collision process has the two components of normal direction and tangential component, as shown in Fig.13. The normal component, F_n , can be determined by viscous damping in a linear contact model as^[38]

$$F_n = k_n d_n - c_n v_n \quad (6)$$

The tangential component, F_t , depends on the force of viscous damping and friction, as shown in^[39]

$$F_t = \min(k_t d_t - c_t v_t, \mu F_n) \quad (7)$$

In Eqs.(6—7), k_n and k_t are the normal and tangential stiffness coefficients, respectively; d , c , and v the overlap zone, the damping coefficients, and the relative velocities, respectively. μ is the friction coefficient, which equals to $\tan\varphi$ in $F_t^{\max} = \mu F_n = F_n \tan\varphi$.

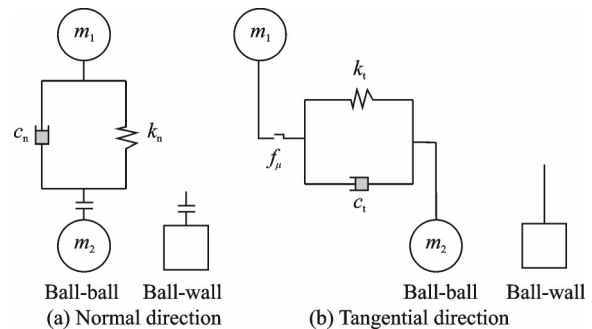


Fig.13 Viscous damping in a linear contact model^[38]

Fig.14 shows F_{mcf} in each group. F_n and F_t are a little changed in the groups 1, 2, 4, 5, 7 and 9; while they obviously increase in the groups 3, 6,

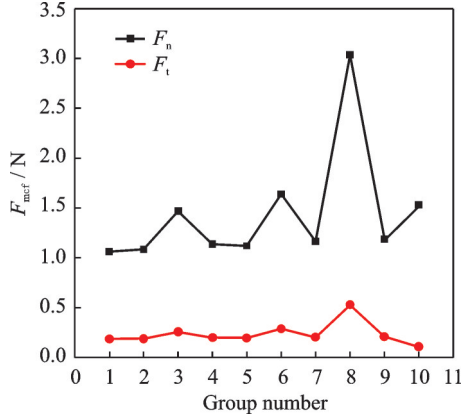


Fig.14 Mean contact force in ten groups

and 8 in which a large vibrating amplitude and frequency are performed. According to Eqs.(6—7), the result can be explained with the gradual increase of amplitude and frequency, leading to a larger space between balls, a shorter time of the single ball-motion, and decreasing the relative velocity; thus, F_n and F_t are increased. Moreover, the maximum value of F_{mcf} in group 8 means that the ball-motion behavior can lead to a significant impact on the friction forces of the ground particles, providing the largest breakage rate of S_i in all groups (Fig.12).

3.2 Collision energy loss

The collision energy loss among balls is originated from damping and friction, which involves the two forms of normal and tangential energy losses. The normal energy loss can be obtained from Eqs.(6,8).

$$E_n = \sum_k F_n \Delta d_n = \sum_k [(k_n d_n - c_n v_n) \cdot v_n \cdot \Delta t] \quad (8)$$

The tangential energy loss can be derived from Eqs.(7,9).

$$E_t = \sum_k F_t \Delta d_t = \sum_k \{ [\min(k_t d_t - c_t v_t), \mu F_n] \cdot v_t \cdot \Delta t \} \quad (9)$$

In Eqs.(8—9), Δt refers to the time-step and k the step. During a complete collision, the overlap zone, $\sum \Delta d_n$, is changed from zero to a maximum and, then, approached zero. So, the elastic strain energy becomes zero when the collision is finished, as

shown in

$$\sum_k k_n d_n \cdot v_n \cdot \Delta t = 0 \quad (10)$$

$$\sum_k k_t d_t \cdot v_t \cdot \Delta t = 0 \quad (11)$$

The total collision energy loss during a complete collision is calculated by^[40]

$$E_{\text{total}} = \sum_k [(F_n \cdot v_n \cdot \Delta t) + (F_t \cdot v_t \cdot \Delta t)] = E_n + E_t \quad (12)$$

Fig.15 shows the collision energy loss, E , in each group. The variation of E is similar to that of F_{mcf} in Fig.14, and F_n is much larger than F_t in Fig.14. While, the normal energy loss, E_n , is much smaller than that of the tangential energy loss, E_t , in Fig.15. It can be seen that although F_n is larger, its contact frequency among balls is lower than that of F_t . Combined with the largest value of particle breakage rate S_i in group 8 in Fig.12, the largest tangential contact force and tangential collision energy loss are observed in group 8 as well, indicating that they may be effectively helpful to break the particles compared to the normal ones in the flutter mill.

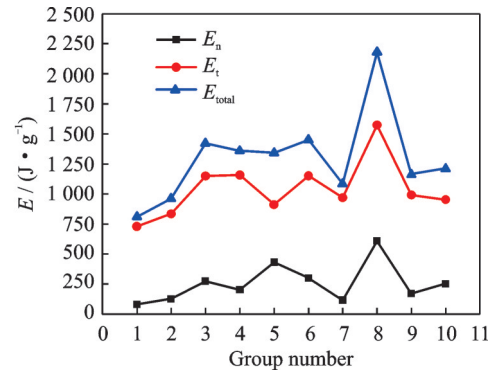


Fig.15 Collision energy loss among balls in ten groups

4 Discussion

From the experimental and numerical results, it can be concluded that the ball-motion behavior in a rotating speed coupled with a high-intensity vibrating is significantly effective to achieve micro-particles owing to the more friction force, F_t , and tangential collision energy, E_t , imposed on the feed particles (as shown in Figs.9, 12, 14 and 15). In

stead, the much lower values of S_i and F_i in group 10 indicate that rotating motion only has been clearly undesirable to accumulate the desired particles finer than 325 mesh. Therefore, the coupled motion is necessary and helpful to change the motion behavior of grinding balls.

In addition, among the combined-motion conditions, group 8 shows a superior crushing performance for the feed particles, not only a larger breakage rate of S_i but also much smaller and more uniform distribution of ground particles, as analyzed in Fig.5 and Table 5.

From Figs.12 and 15 it can be deduced that the curves of E_t or E_n , and S_i change similarly in for mer nine groups. Then, the points in Fig.16 are attempted to express the relationship between E_t (or E_n) and S_i . The points tagged by the squares are ignored because they are obtained in group 10. A linear function is used to fit these points and a relational formula is expressed as

$$S_i = a_1 E_t + b_1 \quad (13)$$

or

$$S_i = a_2 E_n + b_2 \quad (14)$$

where a and b are the constant coefficients with different values for the flutter mill under various motion conditions. According to Eqs.(13—14), S_i can be predicted in some motion conditions and may be compared with the ball-motion behavior of E_n or E_t . Therefore, high-cost, hard-operating, and environment-polluting experiments can be extensively avoided for the flutter mill.

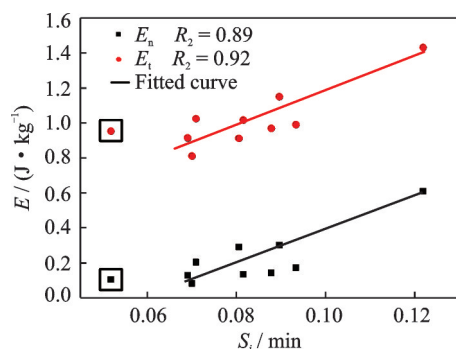


Fig.16 Linear dependence of S_i to E

5 Conclusions

(1) The coupled motions can preferentially accumulate micro-particles compared to the rotating motion only because of the more uniform distribution-size, smaller size of ground particles, larger production rate of micro-particles, F_i , and the bigger particle breakage rate, S_i , in the multiple grinding experiments.

(2) In the coupled motions, it is found that the main role of crushing particles is the tangential force and the tangential collision energy loss, which is different from the traditional one. The optimal crushing performance is obtained in group 8, in which the rotating speed ratio, vibrating amplitude, and frequency are 85%, 8 mm, and 12 Hz, respectively. Therefore, an efficiency way of accumulating micro-particles is successfully achieved.

(3) How the ball-motion behavior influence particle crushing performance is discussed in the flutter mill by combining experimental and numerical analyses. A linear positive correlation is disclosed between particle breakage rate S_i and collision energy loss E .

References

- [1] FUERSTENAU D W, ABOUZEID A Z W. The energy efficiency of ball mill in comminution[J]. International Journal of Mineral Processing, 2012, 67 (1/2/3/4): 161-185.
- [2] ZHENG S L. Industrial mineral powder production in China[J]. China Particology, 2017, 5: 376-383.
- [3] SUN Yi, DONG Mingfeng, MAO Yalang, et al. Analysis on grinding media motion in ball mill by discrete element method[J]. Manufacturing Engineering, Quality and Production Systems, 2009, 1 (1): 227-231. (in Chinese)
- [4] SUN Y, LIANG M, JIN X H, et al. Experimental and modeling study of the regular polygon angle-spiral liner in ball mills[J]. Chinese Journal of Mechanical Engineering, 2017, 30(2): 363-372.
- [5] ZHANG J G, BAI Y, DONG H, et al. Influence of ball size distribution on grinding effect in horizontal planetary ball mill[J]. Advanced Powder Technology, 2014, 25(3): 983-990.

- [6] CLEARY W P, HOYER D. Centrifugal mill charge motion and power draw: Comparison of DEM predictions with experiment[J]. *International Journal of Mineral Processing*, 2010, 59(2): 131-148.
- [7] HE M, WANG Y, FORSBERG E. Parameter effects on wet ultrafine grinding of limestone through slurry rheology in a stirred media mill[J]. *Powder Technology*, 2016, 16: 10-21.
- [8] SHI Guiming, XIAO Qingfei, LUO Chunmei, et al. Study on effect of ball size precision on metallurgical performance of beneficiation[J]. *Metal Mine*, 2017, 1: 55-57. (in Chinese)
- [9] LIANG Man, SUN Yi, JI Pengpeng, et al. Numerical analysis on regular polygon angle-spiral liners design in a ball mill[J]. *Chinese Journal of Mechanical Engineering*, 2015, 51(17): 203-212. (in Chinese)
- [10] TORAMAN O Y, KATIRCIOG L D. A study on the effect of process parameters in stirred ball mill[J]. *Advanced Powder Technology*, 2011, 22: 26-30.
- [11] OUATTARA S, FRANCES C. Grinding of calcite suspensions in a stirred media mill: Effect of operational parameters on the product quality and the specific energy[J]. *Powder Technology*, 2014, 255: 89-97.
- [12] JIANG Xinping, ZHOU Quan, YUAN Feng. Structural strength modeling and analysis of discharge opening of center drive mill[J]. *Journal of Nanjing University of Aeronautics & Astronautics*, 2014, 46(6): 959-962. (in Chinese)
- [13] LIU H Y, YANG Y, LI F S. Study on the equipment and technique of bi-rolling superfine milling[J]. *New Equipment Technology and Application*, 2015, 12: 58-60.
- [14] XU B, WANG S L, LI S J. Dynamic analysis and simulation study[J]. *Chinese Journal of Mechanical Engineering*, 2018, 44(3): 105-109.
- [15] HUANG H, QI L H, ZENG X H, et al. Principle of micro-feeding powders by ultrasonic vibration and influence of amplitude on rate of micro-feeding powders[J]. *Chinese Journal of Mechanical Engineering*, 2019, 45: 267-272.
- [16] HOSSEIN A, MAHMUD A. Influence of processing parameters on grinding mechanism in planetary mill by employing discrete element method[J]. *Advanced Powder Technology*, 2012, 23: 708-716.
- [17] SUN Y, HUANG X H, JIN X H. Numerical analysis of the ball mill coupled with the vertical vibration Frontiers of energy[C]//*Proceedings of Materials and Information Engineering*. Switzerland: *Advanced Materials Research*, 2014: 638-642.
- [18] GUPTA V K, SHARMA S. Analysis of ball mill grinding operation using mill power specific kinetic parameters[J]. *Advanced Powder Technology*, 2014, 25(2): 625-634.
- [19] FAN D F, SUN Y, MAO Y L, et al. Analysis of medium motions under the hybrid motion state in the ball mill[J]. *Mining & Processing Equipment*, 2010, 5: 81-83.
- [20] CLEARY P W. Charge behavior and power consumption in ball mills: Sensitivity to mill operating conditions, liner geometry and charge composition[J]. *International Journal of Mineral Processing*, 2011, 63(2): 79-114.
- [21] POWELL M S, NURICK G N. A study of charge motion in rotary mills. Part 1—Extension of the theory[J]. *Minerals Engineering*, 1996, 9(2): 259-268.
- [22] YING Nan. Research on charge collision energy and grinding performance of flutter ball mill[D]. Hangzhou: Zhejiang University of Technology, 2012. (in Chinese)
- [23] CAO Xueli. Study on influence of media filling rate and ball to powder ratio on the grinding effect of ball mill[D]. Kunming: Kunming University of Science and Technology, 2011. (in Chinese)
- [24] LIANG Man. Influence mechanism of region-character of media motion on ground particles in ball mill[D]. Hangzhou: Zhejiang University of Technology, 2018. (in Chinese)
- [25] WANG M H, YANG R Y, YU A B. DEM investigation of energy distribution and particle breakage in tumbling ball mills[J]. *Powder Technology*, 2012, 223: 83-91.
- [26] YING Nan, SUN Yi, MAO Yalang. Modal analysis and study on flutter ball mill[J]. *Mining & Processing Equipment*, 2012, 40: 58-61. (in Chinese)
- [27] WANG Weitao. The research of grinding media motion in compound movement ball mill and selection of vibration parameters[D]. Hangzhou: Zhejiang University of Technology, 2010. (in Chinese)
- [28] WANG Guoqiang, HAO Wanjun, WANG Jixin. Discrete element method and the practice in EDEM[M]. Xi'an: Northwestern Polytechnic University Press, 2010. (in Chinese)

- [29] WANG C Y, FU X M, TAO Y S, et al. Crushing characteristics of quartz sand under different confining pressures[J]. *Journal of Geological Hazards and Environment Preservation*, 2014, 25: 105-109.
- [30] WU J F, DING Y. Optimization of injection parameters and orthogonal test method based on mold-flow[J]. *Modern Machinery*, 2014, 1: 12-16.
- [31] ZENG Fang, HU Yongping. Particle Technology of Mineral Processing[M]. Xuzhou: China Mining University Press, 2001. (in Chinese)
- [32] HAN Y, YANG Z L, QIAN P, et al. Resolution increase and noise removal in particle size distribution measurement with shift in transform[J]. *Transactions of Nanjing University of Aeronautics and Astronautics*, 2015, 32(4): 446-451.
- [33] MAO Yalang. Modeling nipped breakage mass of particle beds and comminution mechanism of ball mill[D]. Hangzhou: Zhejiang University of Technology, 2016. (in Chinese)
- [34] LIANG Man, SUN Yi, SHAN Jihong. Experiment on the influence of features of the broken particle size in a flutter ball mill[J]. *Chinese Journal of Mechanical Engineering*, 2018, 54(7): 205-215. (in Chinese)
- [35] HERBST J A, FUERSTENAU D W. The zero-order production of fine sizes in comminution and its implications in simulation[J]. *Transactions AIME*, 1968, 241: 538-546.
- [36] LIANG D, HE Z Z, XU L, et al. Effect of particle size distribution on radiative heat transfer in high-temperature homogeneous gas-particle mixtures[J]. *Transactions of Nanjing University of Aeronautics and Astronautics*, 2019, 36(5): 733-746.
- [37] DENIZ V. A study on the specific rate of breakage of cement materials in a laboratory ball mill[J]. *Cement and Concrete Research*, 2013, 33(3): 439-445.
- [38] POWELL M S, MCBRIDE A T. What is required from DEM simulations to model breakage in mill[J]. *Minerals Engineering*, 2006, 19: 1013-1021.
- [39] TUZCU E T, RAJAMANI R K. Modeling breakage rates in mills with impact energy spectra and ultra-fast load cell data[J]. *Minerals Engineering*, 2011, 24(3): 252-260.
- [40] SABAH E, ÖZDEMİR O, KOLTKA S. Effect of ball mill grinding parameters of hydrated lime fine grinding on consumed energy[J]. *Advanced Powder Technology*, 2013, 24(3): 647-652.

Acknowledgements This work was supported in part by the National Natural Science Foundation of China (Nos. 51675484, 51275474) and Zhejiang Provincial Natural Science Foundation of China (No.LZ12E05002). The authors would like to acknowledge the following people for their assistance: Mr. XIANG Jingcheng, Dr. JIN Xiaohang, Mr. HUANG Shaowei, and Mr. XU Peng, all with the Key Laboratory of Special Equipment Manufacturing and Advanced Processing technology, Ministry of Education, Zhejiang University of Technology.

Authors Dr. LIANG Man received the B.S. degree in electromechanical engineering from China Jiliang University in 2012 and the Ph.D. degree in mechanics engineering from Zhejiang University of Technology in 2018, respectively. She joined in China Jiliang University in April 2018, where she is a lecturer of College of Mechanical and Electrical Engineering. Her research is focused on mechanical design, system detection, manufacturing and optimization.

Prof. SUN Yi received the B.S. degree in mechanics from Beijing University of Aeronautics and Astronautics in 1993 and the Ph.D. degree from Zhejiang University in 2007. He is currently a professor at College of Mechanical Engineering, Zhejiang University of Technology, Hangzhou, China. His research has focused on mechanical design and optimization, and integration system of manufacturing.

Author contributions Dr. LIANG Man designed the study, compiled the models, conducted the experiment, interpreted the results and wrote the manuscript. Prof. SUN Weihong gave critical discussions and background of the study, and revised the manuscript. Prof. SUN Yi offered the main idea and guided the preparation of the grinding experiment. Mr. SHAN Jihong assisted with sampling and laboratory analyses. All authors commented on the manuscript draft and approved the submission.

Competing interests The authors declare no competing interests.

颤振球磨机中介质运动行为对颗粒破碎效果的影响及微细颗粒制备方法

梁 曼¹, 孙卫红¹, 孙 毅², 单继宏²

(1. 中国计量大学机电工程学院, 杭州 310018, 中国; 2. 浙江工业大学机械工程学院, 杭州 310014, 中国)

摘要: 介质球的运动状态对提升微细颗粒的破碎效果具有重要作用。本文提出一种通过改变球磨过程中介质球运动状态制备微细颗粒的方法, 并开展多组不同运动状态的粉磨试验研究, 探讨颗粒群的破碎参数, 如破碎率 S_i 、微细颗粒产率 F_i 和单位介质球微细颗粒产率 F_i^* 等在不同运动工况下的幅值变化。试验结果显示: 在颤振复合球磨运动中, 当磨机转速率为 85%、振幅为 8 mm、频率为 12 Hz 时, 微细颗粒的破碎率和制备效率最优。同时讨论了介质球运动形态参数与微细颗粒破碎效应的内在关联, 得到介质球碰撞能 E 与微细颗粒破碎率 S_i 的关系式。因此, 本文不仅提供了一种制备微细颗粒的有效方法, 而且揭示了颤振复合球磨运动中介质球运动形态是如何影响颗粒破碎效应的。

关键词: 颤振球磨机; 磨介运动形态; 破碎率; 碰撞能损失; 微细颗粒制备